Experimental Astronomy (2024) 57:8
https://doi.org/10.1007/s10686-024-09927-x

RESEARCH

Design and characterization of a 90 GHz CMB TES bolometer

Yu Xu[1,2] · Zhengwei Li[1] · Yongping Li[1,3] · Yifei Zhang[1] · Xufang Li[1] · Xuefeng Lu[1] · Guofu Liao[1,2] · Qingchen Li[4] · Fangjun Lu[1] · Laiyu Zhang[1] · Yudong Gu[1] · Zhouhui Liu[1] · Shibo Shu[1] · Zhi Chang[1] · Guofeng Wang[1] · Yongjie Zhang[1] · He Gao[1] · Aimei Zhang[1] · Daikang Yan[1] · Congzhan Liu[1]

Received: 26 November 2023 / Accepted: 9 February 2024

Abstract
The transition-edge sensor (TES) as a type of low-temperature superconducting detector offers superior sensitivity due to its low thermal noise. In this work, we present a prototype TES bolometer designed for cosmic microwave background (CMB) polarization measurements. This TES is made of aluminum doped with a low concentration of manganese (2000 ppm by atomic percentage), and is deposited on the SiNx membrane which connects to the silicon substrate via narrow legs. In order to calculate its electrothermal parameters we have performed dark characterizations, which include measuring voltage-current (IV) curve at different bath temperatures, square-wave time response at various bias voltages, and noise level. This TES bolometer shows a noise equivalent power (NEP) of about 5×10^{-17} W/$\sqrt{\text{Hz}}$, which meets the requirement of CMB observation. However, its saturation power is smaller and time constant is larger than what are expected. We have analyzed the reasons and will make corresponding improvements in our future work.

Keywords Cosmic microwave background · Superconducting transition edge sensor · Bolometer

1 Introduction

CMB is the radiation remnant from the Big Bang, pervading the entire universe and containing rich information about the early stages of the universe. Measurements of the CMB offer significant insights into various aspects, including inflation, neutrinos, dark matter, dark energy, etc. TESs have consistently demonstrated reliable performance and made substantial contributions to research on the CMB. The current operational

✉ Daikang Yan
yandk@ihep.ac.cn

Extended author information available on the last page of the article

Published online: 02 March 2024

CMB telescopes, including Advanced ACTPol [1], CLASS [2], and SPTpol [3], all utilize TESs as their focal plane detector. For ground-based CMB telescopes, various observation windows are designated based on the absorption of photons by oxygen and water in the atmosphere. Among these, the 90 GHz observation window exhibits the least contamination [4]. However, single-frequency observations of the CMB face challenges due to foreground contamination from sources like synchrotron radiation and galactic dust. To address this issue, TESs are specifically designed to observe the polarization of the CMB across multiple frequency bands. This allows for the efficient removal of foreground signals [4]. Here, we have designed a single-pixel dual polarized TES for 90 GHz CMB observation and evaluated its dark performance.

The TES is biased in the superconducting transition region with a constant voltage [5]. When the incident energy is absorbed by the TES, it is converted into heat, leading to an increase in the resistance of the TES. The voltage bias results in a decrease in Joule power. Meanwhile the cooling power from the heat sink remains constant, leading to the TES returning to its original state in the absence of energy incidence. A schematic diagram illustrating this concept is presented in Fig. 1.

2 The detector design

The structure of our polarization-sensitive TES bolometer is depicted in Fig. 2. In the middle of the pixel, there are two pairs of orthomode transducer (OMT) coupling probes, each pair dedicated to an orthogonal linear polarization direction. The OMT polarizes the signal received by the feedhorn antenna and couples it to the coplanar waveguide (CPW). The signal is then transmitted to the microstrip line through an impedance matching conversion section. The signal passes through a 90 GHz stub filter to reach the island, which has a weak thermal connection with the cold bath through a set of four SiNx legs. On the island, the signal is converted into heat, which is absorbed and detected by the AlMn TES bolometer. Within each pixel, there are two optical TESs, each one dedicated to a linear polarization direction. Additionally, there are two dark TESs which are not coupled to the OMT and are used to compare with the signal response of the optical TESs. A superconducting quantum interference device (SQUID) readout system is used to measure the current signal of the TES [6].

The design of microwave devices is achieved by utilizing HFSS® [7] software for simulation and optimization. We design the TES for a future small-aperture CMB telescope at Ali area, China. Given the precipitable water vapor (PWV) of the observation site, the observed frequency band, and the internal power, we have estimated the total load power to be 6.9 pW [8]. To enhance the linearity of the TES, we aim for a saturation power (P_{sat}) of 14 pW, about twice the load power [8]. We define P_{sat} as the power value that drives the TES in its transition from its superconducting state to 50% of normal resistance (R_n), which can be described by the following equation [9]:

$$P_{sat} = \frac{G}{nT_c^{n-1}}(T_c^n - T_b^n), \tag{1}$$

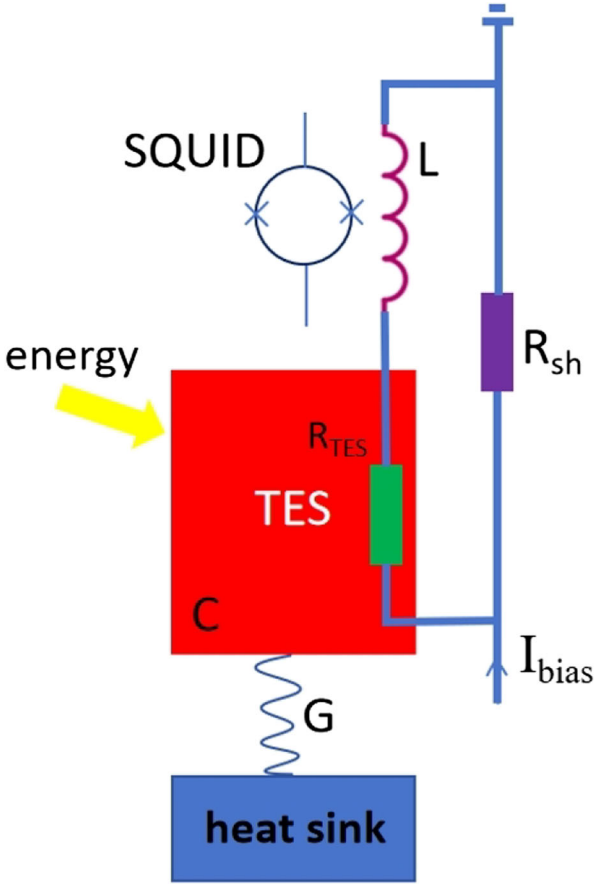

Fig. 1 Negative electrothermal feedback of TES. A bias current I_{bias} is applied to a shunt resistor R_{sh} in parallel with an inductance L (including both SQUID and stray inductance) and a TES C with resistance R_{TES}. The TES is connected to the heat sink by a weak thermal link G

where n is the thermal conduction exponent, dependent on the dominant heat transfer mechanism in the material. For materials where phonon heat transfer is the primary mechanism, n typically ranges between 3 and 4. For materials where electron heat transfer is dominant, n is approximately 2 [10]. When designing, the n for SiNx is assumed to be 3. The bath temperature, T_b, is determined by the performance of the refrigerator. To minimize thermal noise [11], the superconducting transition temperature (T_c is the temperature at half of the TES's normal resistance) of the TES is set to 500 mK and can be adjusted by tuning the concentration of Mn and employing a baking process [12]. The thermal conductance, denoted as G, is calculated to be 90 pW/K using Eq. (1). The thermal conductance can be controlled by adjusting the length and cross-sectional area of the leg [13].

To ensure proper speed matching with the readout electronics, we set the natural time constant (τ_{nat}) of the TES to 10 milliseconds. This time constant is determined by

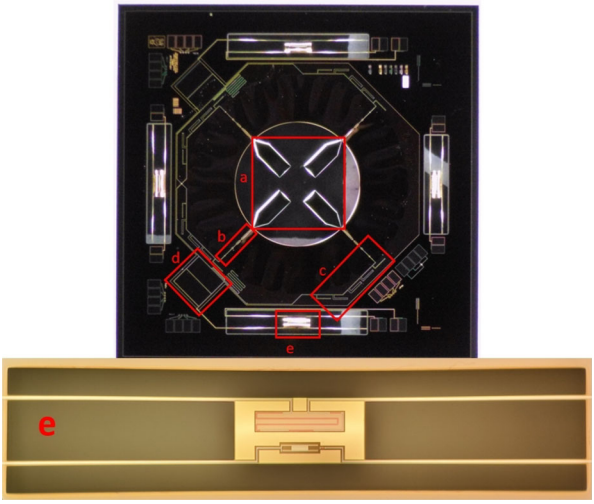

Fig. 2 Structure of single-pixel dual-polarized 90 GHz TES. (a) OMT. (b) CPW-MS impedance matching conversion section. (c) 90 GHz stub filter. (d) hybrid-tee which adds signals from two opposing fins. (e) TES thermal island

the geometric properties of the island, specifically $\tau_{nat} = C/G$, where C represents the heat capacity of the bolometer, which is calculated to be 0.9 pJ/K. The heat capacity is adjusted by manipulating the volume of thermal ballast on the suspended island. When operating under negative electrothermal feedback, the TES exhibits both electrical and effective thermal time constants. The electrical time constant, τ_{el}, is determined by the TES bias circuit elements and its current sensitivity. The effective thermal time constant, τ_{eff}, is slower than τ_{el}. And therefore, it determines the bolometer's response speed to changes in the sky loading. The effective thermal time constant can be represented by the 3dB frequency, f_{3dB} [14],

$$f_{3dB} = \frac{1}{2\pi\tau_{eff}} = \frac{G}{2\pi C}(1 + \frac{1}{1+\beta}\frac{\alpha P_{bias}}{T_c G}), \tag{2}$$

In the equation, $\alpha = d\log R/d\log T$ represents the TES sensitivity of resistance to temperature, $\beta = d\log R/d\log I$ represents the TES sensitivity of resistance to current, and P_{bias} represents the electrical bias power applied to the TES [9]. In Section 3, we measure f_{3dB} to deduce the C of the TES bolometer.

Another important performance of TES bolometer is noise level. The noise primarily consists of thermal fluctuation noise, resistor thermal noise, and amplifier noise. The dominant noise source at the TES working state is phonon noise resulting from temperature fluctuations. This phonon noise can be expressed in terms of NEP as [10]:

$$(\text{NEP})^2 = 4k_B G T_c^2 \gamma, \tag{3}$$

Here, k_B represents Boltzmann's constant, and $\gamma \approx 0.71$ is a parameter determined by the weak heat link structure [10]. The theoretical NEP is calculated

to be $3 \times 10^{-17}\mathrm{W}/\sqrt{\mathrm{Hz}}$, which meets the observation requirement (smaller than $5 \times 10^{-17}\mathrm{W}/\sqrt{\mathrm{Hz}}$) [9].

3 Characterization and analysis

In order to determine the saturation power, an IV test was executed. The characterization process involved the use of an adiabatic demagnetization refrigerator (ADR) and SQUID electronics. The TES chip is clamped to a copper sample box which is thermally anchored to the 50 mK FAA (Ferric Ammonium Alum) stage of the ADR and enclosed within a niobium cylinder to provide magnetic shielding. A current source is employed to supply bias current I_{bias} to the TES. The current flowing through the TES is measured by a SQUID amplifier.

We accomplished IV curve measurements at various bath temperatures ranging from 150 to 500 mK every 10 mK. Figure 3 shows eight representative IV curves for clarity. By fitting the data as depicted in Fig. 4 using Eq. (1), we obtained the following parameter values: G = 30.4 pW/K, T_c = 500.2 mK, and n = 2.7. Notably, the thermal conductance is smaller than the design value, which could potentially be attributed to surface damage on the SiNx legs during the back etching process. In future fabrication, we plan to add a silicon dioxide layer under the SiNx layer to protect the SiNx surface from the deep reactive ion etching process and to enhance the phonon transportation within the SiNx layer through interface reflection. The saturation power is also smaller

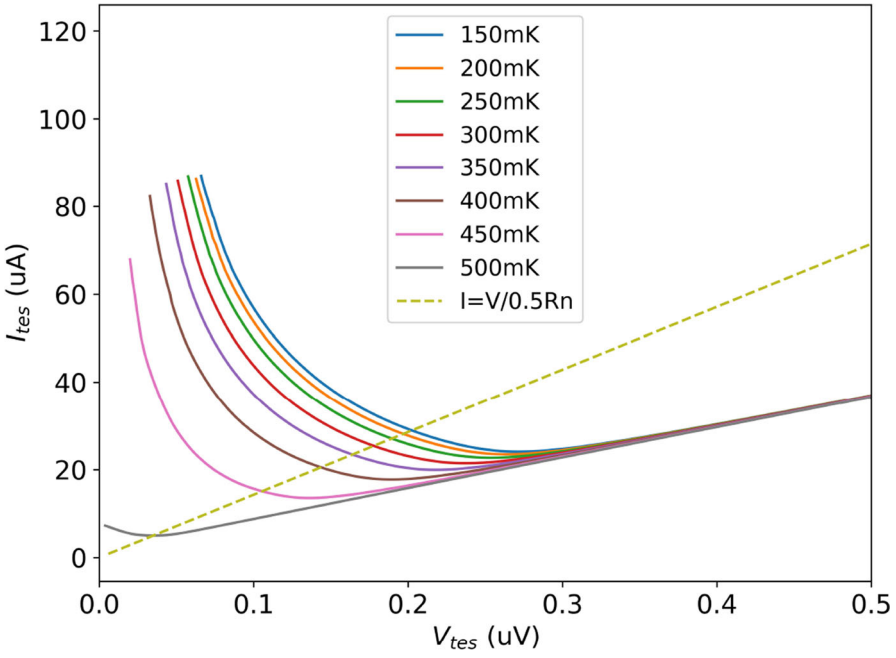

Fig. 3 IV curves measured at various bath temperatures ranging from 150 to 500 mK

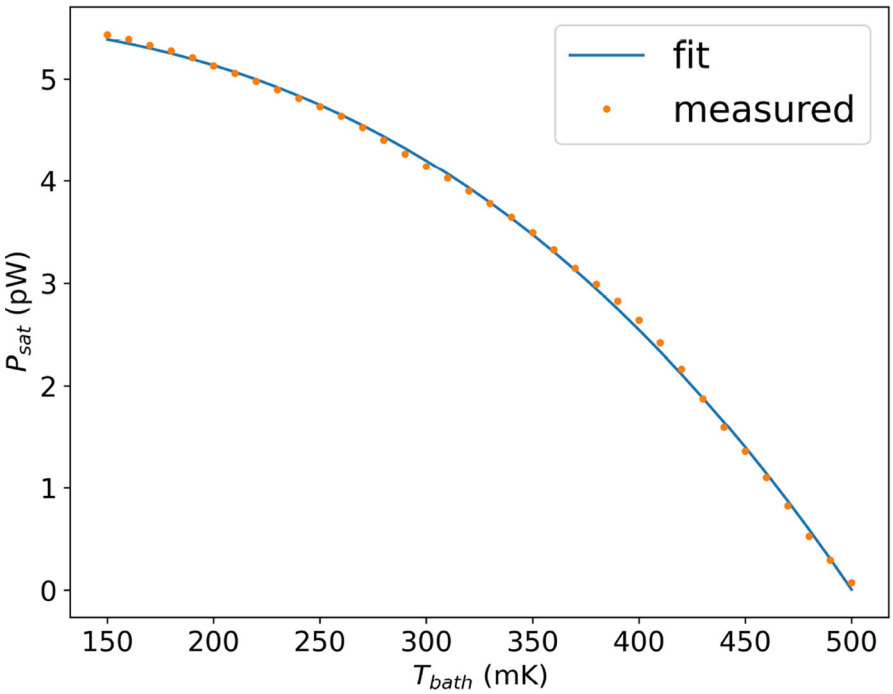

Fig. 4 Fit saturation power using Eq. (1)

than the desired value. As indicated by Eq. (1), it can be directly improved by increasing G in our future fabrication.

To determine the time constant, we performed square wave tests. A small square wave was added to the voltage bias applied to the detectors [15]. To avoid the TES bias resistance shifting too far while applying the additional AC signal, the amplitude of the square wave is limited to be smaller than 5% of the DC bias voltage. The TES is biased and at different $\%R_n$ values at various bath temperatures, and the measurements are taken with a sampling rate of 0.1 MHz.

In Fig. 5, we show an example of the bias step time stream in DAC units. Each step is fitted to a single pole exponential function of the form $f(t) = Ae^{-t/\tau_{eff}} + C$. Care is taken to choose the starting point of the fit in order to primarily capture the thermal response rather than the electrical response. The exponential decay fit begin at the asymptotic value of the previous step. The fitting line is plotted in Fig. 6. Figure 7 shows the time constants in f_{3dB} at different bias power and fraction of normal resistance. We assume that within a narrow bias range $0.5R_n$-$0.8R_n$, the value of $\alpha/(1+\beta)$ remains constant. Then Eq. (2) can be simplified to the following form:

$$f_{3dB} = 1/2\pi\tau_{nat} + BP_{bias}, \tag{4}$$

The natural time constant, τ_{nat}, which corresponds to the bolometer time constant without negative electrothermal feedback, was extrapolated with Eq. (4) from the

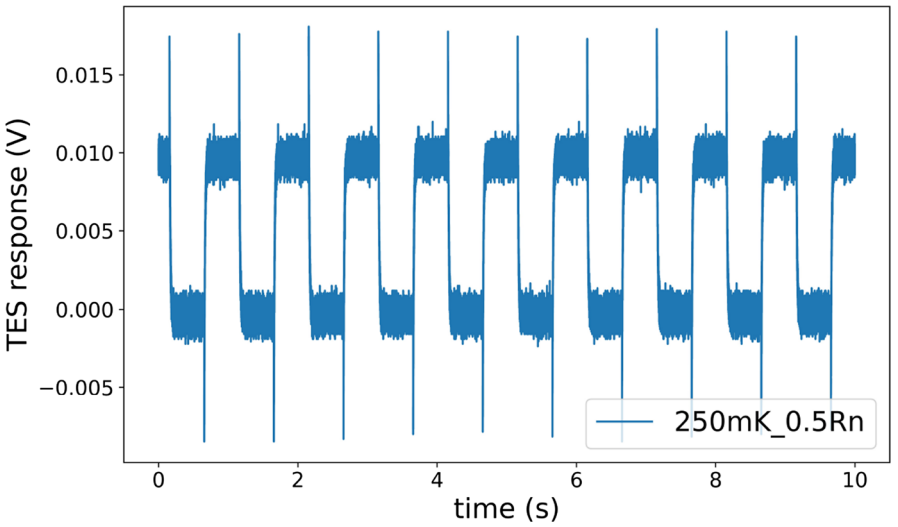

Fig. 5 Example bias step time stream in DAC units

value of f_{3dB} at zero power. The fitting line intersects at 2 Hz at zero bias power. We calculated that $\tau_{nat} = 79.6$ milliseconds. With the G value calculated from the previous IV measurement, we obtain that C = 2.4 pJ/K. This value is more than twice of the designed value. In the next version of design, we plan to reduce the thickness of the gold in order to decrease heat capacity.

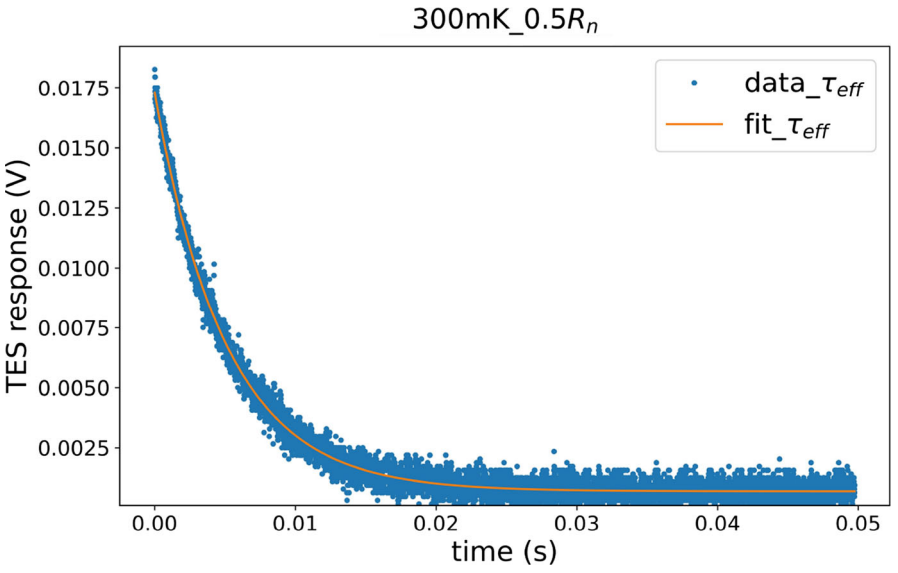

Fig. 6 Fit time constant

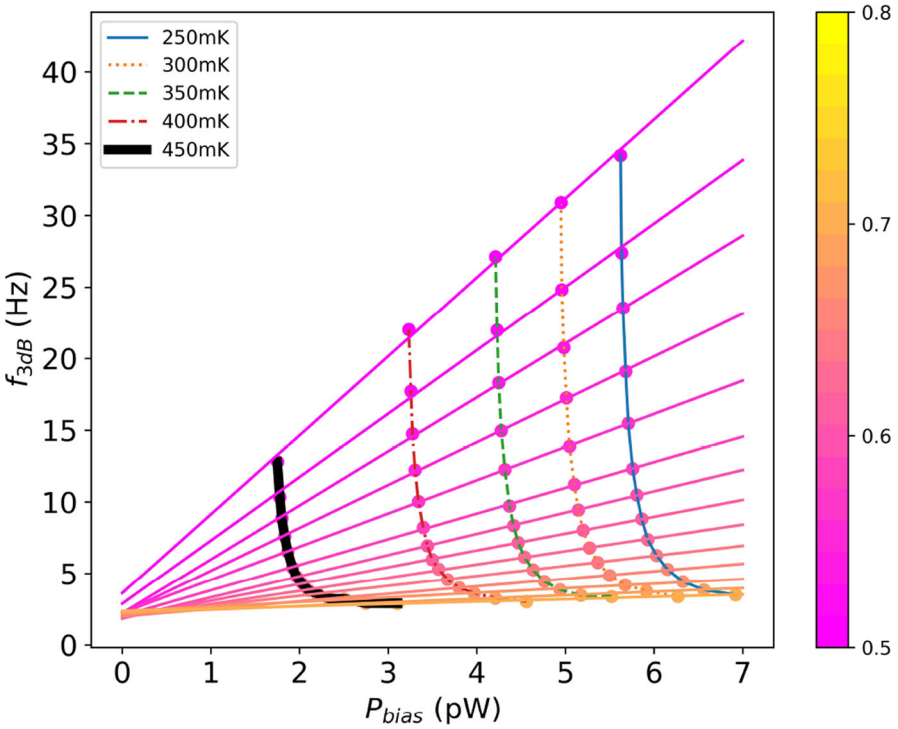

Fig. 7 Bias step time constants as a function of bias power and $\%R_n$ at different bath temperatures. The colorbar represent the different resistance

Dark measurements in the laboratory are valuable for assessing the noise characteristics of the TES. We measured the output with a sampling rate of 0.5 MHz for 10 seconds at different $\%R_n$ values at a bath temperature of 300 mK. Figure 8 demon-

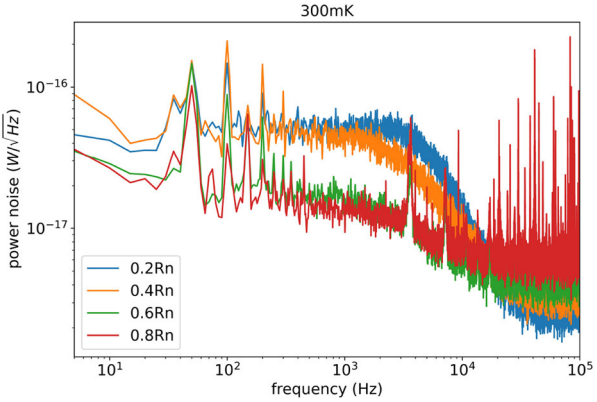

Fig. 8 The power noise of the TES at various bias points across the transition region, at a bath temperature of 300 mK. The power noise is the noise equivalent current multiplied by TES bias voltage

strates that the NEP values are smaller than $5 \times 10^{-17}\mathrm{W}/\sqrt{\mathrm{Hz}}$. However the noise value is still higher than theoretical expectation, and the origin of the excess noise will be studied in our future work.

4 Conclusion and future work

In summary, we developed a 90 GHz TES bolometer for CMB observation. The measured thermal conductance is 30.4 pW/K, heat capacity is 2.4 pJ/K. In future fabrication, we plan to add a silicon dioxide layer under the SiNx layer to protect the SiNx surface and reduce the thickness of the gold to correct thermal conductance and the heat capacity, respectively. The NEP meets the observation requirement. In the next step, we will conduct measurements to assess the optical performance of this TES bolometer.

Acknowledgements The authors would like to thank Dr.Guanhua Gao for his contribution to fabrication.

Author Contributions Zhengwei Li arranged the experiment routine. Yongping Li and Xufang Li helped in data acquisition and analysis. Yu Xu and Daikang Yan did the experiment, analyzed data in detail and wrote the main manuscript text. All authors reviewed the manuscript.

Funding This work is supported by the National Key Research and Development Program of China (Grant No. 2022YFC2205000, No. 2020YFC2201604, No. 2022YFC2205002, No. 2021YFC2203400).

Data Availability No datasets were generated or analysed during the current study.

Declarations

Competing interests The authors declare no competing interests.

References

1. Li, D., Austermann, J.E., Beall, J.A., Becker, D.T., Duff, S.M., Gallardo, P.A., Henderson, S.W., Hilton, G.C., Ho, S.-P., Hubmayr, J., et al.: Almn transition edge sensors for advanced actpol. J. Low Temp. Phys. **184**, 66–73 (2016)
2. Rostem, K., Ali, A., Appel, J.W., Bennett, C.L., Brown, A., Chang, M.-P., Chuss, D.T., Colazo, F.A., Costen, N., Denis, K.L., et al.: Silicon-based antenna-coupled polarization-sensitive millimeter-wave bolometer arrays for cosmic microwave background instruments. In: Millimeter, Submillimeter, and Far-Infrared Detectors and Instrumentation for Astronomy VIII, vol. 9914, pp. 54–63 (2016). SPIE
3. Schmidt, D.R., Cho, H.-M., Hubmayr, J., Lowell, P., Niemack, M.D., O'Neil, G.C., Ullom, J.N., Yoon, K.W., Irwin, K.D., Holzapfel, W., et al.: Al-mn transition edge sensors for cosmic microwave background polarimeters. IEEE Trans. Appl. Supercond. **21**(3), 196–198 (2010)
4. Abazajian, K.N.: Cmb-s4 science book, first edition. (2016) https://doi.org/10.2172/1352047
5. Lee, A.T., Richards, P.L., Nam, S.W., Cabrera, B., Irwin, K.D.: A superconducting bolometer with strong electrothermal feedback. Appl. Phys. Lett. **69**(12), 1801–1803 (1996). https://doi.org/10.1063/1.117491
6. Clarke, J., Braginski, A.I.: The SQUID Handbook: Fundamentals and Technology of SQUIDs and SQUID Systems, Volume I. The SQUID Handbook: Fundamentals and Technology of SQUIDs and SQUID Systems, Volume I, ??? (2005)
7. ANSYS®: Release 17.2, ANSYS Inc. http://www.ansys.com

8. Gao, H., Liu, C., Li, Z., Liu, Y., Li, Y., Li, S., Li, H., Gao, G., Lu, F., Zhang, X.: Introduction to the detection technology of ali cmb polarization telescope. Radiation Detection Technology and Methods. **1**, 1–10 (2017)
9. Irwin, K.D., Hilton, G.C.: Transition-edge sensors. Cryogenic Particle Detection. 99 (2005)
10. Mather, J.C.: Bolometer noise: nonequilibrium theory. Appl. Opt. **21**(6), 1125–1129 (1982)
11. Arnold, K.S.: Design and deployment of the polarbear cosmic microwave background polarization experiment. PhD thesis, University of California, Berkeley. (2010)
12. Niemack, Michael, D., Simon, Sara, M., Beall, James, A., Lanen, V., Jeff, Becker, Daniel, T.: Almn transition edge sensors for advanced actpol
13. Guan-Hua, G., Yu, X., Guo-Fu, L., Fang-Jun, L.: Estimation method for beam size of superconducting transition edge detector. Acta Phys. Sin. **71**(15), 158502 (2022). https://doi.org/10.7498/aps.71.20220335
14. Cothard, N.F., Ali, A.M., Austermann, J.E., Choi, S.K., Xu, Z.: Comparing complex impedance and bias step measurements of Simons Observatory transition edge sensors (2020)
15. Stever, S.L., Couchot, F., Sauvage, V., Coron, N.: Benefits of bolometer Joule stepping and Joule pulsing. J. Low Temp. Phys. **199**, 110–117 (2019)

Authors and Affiliations

Yu Xu[1,2] · Zhengwei Li[1] · Yongping Li[1,3] · Yifei Zhang[1] · Xufang Li[1] · Xuefeng Lu[1] · Guofu Liao[1,2] · Qingchen Li[4] · Fangjun Lu[1] · Laiyu Zhang[1] · Yudong Gu[1] · Zhouhui Liu[1] · Shibo Shu[1] · Zhi Chang[1] · Guofeng Wang[1] · Yongjie Zhang[1] · He Gao[1] · Aimei Zhang[1] · Daikang Yan[1] · Congzhan Liu[1]

Yu Xu
xuyu97@ihep.ac.cn

Zhengwei Li
lizw@ihep.ac.cn

Yongping Li
liyp@ihep.ac.cn

Yifei Zhang
zhangyf@ihep.ac.cn

Xufang Li
lixufang@ihep.ac.cn

Xuefeng Lu
luxf@ihep.ac.cn

Guofu Liao
liaoguofu@ihep.ac.cn

Qingchen Li
liqcquantum@163.com

Fangjun Lu
lufj@ihep.ac.cn

Laiyu Zhang
zhangly@ihep.ac.cn

Yudong Gu
guyd@ihep.ac.cn

Zhouhui Liu
liuzh@ihep.ac.cn

Shibo Shu
shusb@ihep.ac.cn

Zhi Chang
changzhi@ihep.ac.cn

Guofeng Wang
wanggf@ihep.ac.cn

Yongjie Zhang
zhangyj@ihep.ac.cn

He Gao
hgao@ihep.ac.cn

Aimei Zhang
zhangam@ihep.ac.cn

Congzhan Liu
liucz@ihep.ac.cn

[1] Key Laboratory of Particle Astrophysics, Institute of High Energy Physics, CAS, 19B Yuquan Road, Shijingshan District 100049, Beijing, China

[2] School of Physical Science, University of Chinese Academy of Sciences, 19A Yuquan Road, Shijingshan District 100049, Beijing, China

[3] Spallation Neutron Source Science Center, Institute of High Energy Physics, CAS, 1 Zhongziyuan Road, Dongguan 523803, Guangdong, China

[4] Institute of Frontier and Interdisciplinary Science, Shandong University, 72 Binhai Road, Jimo District, Qingdao 266237, Shandong, China